

A Combined Pulse EPR and Monte Carlo Simulation Study Provides Molecular Insight on Peptide–Membrane Interactions

Michal Gordon-Grossman,^{†,‡} Yana Gofman,^{‡,§,||} Herbert Zimmermann,[‡] Veronica Frydman,[#] Yechiel Shai,[∇] Nir Ben-Tal,^{*,||} and Daniella Goldfarb^{*,†}

Departments of Chemical Physics, Chemical Infrastructure Unit, Biological Chemistry, The Weizmann Institute of Science, Rehovot, Israel 76100, GKSS Research Center, Geesthacht, Germany 21502, Max-Planck Institute for Medical Research, Heidelberg, Germany, and Department of Biochemistry, The George S. Wise Faculty of Life Sciences, Tel-Aviv University, Tel-Aviv, Israel 69978

Received: June 1, 2009; Revised Manuscript Received: July 28, 2009

We present a new approach to obtain details on the distribution and average structure and locations of membrane-associated peptides. The approach combines (i) pulse double electron–electron resonance (DEER) to determine intramolecular distances between residues in spin labeled peptides, (ii) electron spin echo envelope modulation (ESEEM) experiments to measure water exposure and the direct interaction of spin labeled peptides with deuterium nuclei on the phospholipid molecules, and (iii) Monte Carlo (MC) simulations to derive the peptide–membrane populations, energetics, and average conformation of the native peptide and mutants mimicking the spin labeling. To demonstrate the approach, we investigated the membrane-bound and solution state of the well-known antimicrobial peptide melittin, used as a model system. A good agreement was obtained between the experimental results and the MC simulations regarding the distribution of distances between the labeled amino acids, the side chain mobility, and the peptide’s orientation. A good agreement in the extent of membrane penetration of amino acids in the peptide core was obtained as well, but the EPR data reported a somewhat deeper membrane penetration of the termini compared to the simulations. Overall, melittin adsorbed on the membrane surface, in a monomeric state, as an amphipatic helix with its hydrophobic residues in the hydrocarbon region of the membrane and its charged and polar residues in the lipid headgroup region.

Introduction

Key biological processes involve interactions between peptides and the cell membrane, and many biophysical approaches have been used to characterize these interactions. One of the prominent methods used to this end is electron paramagnetic resonance (EPR) spectroscopy. The EPR measurements are based on site directed spin labeling,^{1–3} where a nitroxide side chain, like methanethiosulfonate (MTSL), is introduced at a desired site in the protein/peptide via cysteine substitution mutagenesis. Spin labels can also be attached to phospholipid molecules, thus allowing the examination of changes in membrane ordering and fluidity upon the introduction of a peptide/protein.⁴ The line shape of the EPR spectrum of nitroxide radicals is highly sensitive to the degree of the side chain mobility, whereas the nitrogen hyperfine coupling and the *g*-values, particularly the *g*_{xx} component, sense the polarity^{2,3} and proticity of its close environment.⁵ In addition, increased relaxation rates due to the presence of paramagnetic quenchers provide information about the solvent accessibility and the insertion depth in membranes.^{2,6–8} Additional broadening due

to the introduction of a second spin label provides distance information in the range 7–20 Å.^{3,9,10} The analysis of the accessibility, mobility, and polarity measurements is well established and can be used to reveal the secondary structure and the general location and orientation of the peptide relative to the membrane.^{2,11}

Pulse double electron–electron resonance (DEER) measurements extend the distances accessible by EPR methods to 70 Å,^{12–14} and have been applied in a number of investigations of peptide/protein–membrane interactions.^{15–20} Electron spin echo envelope modulation (ESEEM) is yet another well established technique designed to measure weak hyperfine interactions between unpaired electrons and nearby nuclei that can be further interpreted in terms of distances.^{21–23} Although it is a technique commonly used in studies of the coordination shells of metal ions, it has been scarcely applied in the context of protein/peptide–membrane interactions. Recently, ESEEM has been used to derive the water penetration depth in membranes.^{16,24,25} We have previously shown that peptide–membrane interactions can be identified by combining ESEEM induced by D₂O and ²H in specifically labeled lipid molecules.²⁶ In that preliminary study, which was a proof of principle, the peptides were labeled in one position only.

While EPR techniques provide a wealth of structural information, they do not give directly the atomic level structure but rather provide constraints that can be correlated or combined with modeling techniques. Monte Carlo (MC) simulations have been previously demonstrated to be an important tool in the investigation of peptide–membrane interactions.^{27–34} Typically, the MC methods are based on a reduced representation, which enables comprehensive sampling of peptide conformations and

* Corresponding authors. E-mail: Daniella.goldfarb@weizmann.ac.il (D.G.); NirB@tauex.tau.ac.il (N.B.-T.).

[†] Department of Chemical Physics, The Weizmann Institute of Science.

[‡] Michal Gordon-Grossman and Yana Gofman contributed equally to this work.

[§] GKSS Research Center.

^{||} Tel-Aviv University.

[‡] Max-Planck Institute for Medical Research.

[#] Department of Chemical Infrastructure Unit, The Weizmann Institute of Science.

[∇] Department of Biological Chemistry, The Weizmann Institute of Science.

locations in the membrane in an accelerated manner. This approach allows overcoming the current limited computer power, which often restricts molecular dynamics (MD) simulations, another computational tool often used in the research of the interactions of peptides with lipid bilayers.

In this work, we combined EPR experiments, CW-EPR, ESEEM, and DEER with MC simulations to explore peptide–membrane interactions in molecular detail. To demonstrate the effectiveness of the new approach, we chose melittin, a commonly used model for the investigation of peptide–membrane interactions. We studied its interactions with large unilamellar vesicles (LUVs), consisting of the zwitterionic dipalmitoylphosphatidylcholine (DPPC) and monovalent ion phosphatidylglycerol (PG) at 7:3 molecular ratio. The MC simulations were used to rationalize the experimental results and help in their interpretation on the one hand, and the experimental results served as tests for the predictive power of the simulations on the other. The MC protocol we employed has been developed, tested, and used to study the membrane interactions of peptides, such as magainin2, penetratine,³⁵ and the M2 δ transmembrane segment from the acetylcholine receptor subunit.³⁶ The simulations were carried out both on native and mutated melittin, corresponding to the experiments, in order to determine their structure and orientation in both water and membrane and to elucidate any effect of the spin labeling on the structure.

Melittin, a 26-residue antimicrobial peptide, is the major component of honeybee (*Apis mellifera*) venom.³⁷ The structure of melittin has been investigated under various conditions using X-ray crystallography^{38,39} and NMR (nuclear magnetic resonance) techniques.^{40–43} The crystal structure shows that the peptide forms a tetramer, with each subunit comprising two α -helical segments connected by a hinge at residues 11 and 12 with a kink of $\sim 120^\circ$.³⁹ Apolar residues forming the core of the tetramer are almost completely shielded from the solvent by the hydrophilic side chains and the polypeptide backbones. NMR studies of melittin bound to dodecylphosphocholine (DPC) micelles revealed a rod-like α -helical conformation similar to the crystal structure.^{40,41}

In spite of the significant number of studies examining the orientation of melittin within the membrane, it is still a controversial subject. It was observed that melittin's orientation is affected by various factors. Melittin can be oriented either perpendicular or parallel to the membrane surface, depending on pH, temperature, phospholipid composition, and peptide concentration.⁴⁴ Several studies showed that melittin can adopt a surface-parallel, transmembrane, or pseudotransmembrane orientation in neutral membranes (discussed in ref 44). By contrast, only surface orientation was observed in membranes containing negatively charged lipids.⁴⁴ The surface orientation of melittin is characterized by apolar residues facing the hydrophobic core of the membrane and polar residues facing the aqueous phase.^{40,41}

Our results showed that, upon membrane binding, melittin undergoes conformational changes from a primarily random coil, with some helical content at the C-terminus, to a helical structure. We also show that at low concentrations melittin is oriented parallel to the membrane surface. Examination of specific residue location revealed that all the charged (and highly polar) residues are exposed to the aqueous phase, while hydrophobic amino acids are immersed in the membrane, as anticipated on the basis of empirical data. The distances between the labels measured by DEER and the membrane-penetration depth of the residues in the peptide core, determined by ESEEM, correlated well with the MC simulations. However, melittin's

TABLE 1: Peptide Designations and Sequences^a

sequence	peptide designation
GIGAVLKVLTTGLPALISWIKRKRQQ	Melittin
<u>C</u> GIGAVLKVLTTGLPALISWIKRKRQQ	mel-N
G <u>I</u> C <u>A</u> VLKVLTTGLPALISWIKRKRQQ	mel-C ₃
GIGAVLKVLTTGLPCLISWIKRKRQQ	mel-C ₁₅
GIGAVLKVLTTGLPALICWIKRKRQQ	mel-C ₁₈
GIGAVLKVLTTGLPALISWIKRKRQQ <u>C</u>	mel-C ₂₇
<u>C</u> GIGAVLKVLTTGLPCLISWIKRKRQQ	mel-NC ₁₅
GIGAVLKVLTTGLPCLISWIKRKRQQ <u>C</u>	mel-C ₁₅ C ₂₇
GICAVLKVLTTGLPALICWIKRKRQQ	mel-C ₃ C ₁₈
<u>C</u> GIGAVLKVLTTGLPALISWIKRKRQQ <u>C</u>	mel-NC ₂₇

^a The position of the spin label is indicated by C.

termini were found to penetrate somewhat deeper into the membrane than predicted by the MC simulations.

Experimental Methods

Materials. The phospholipids dipalmitoylphosphatidylcholine (DPPC) (Sigma) and egg phosphatidylglycerol (PG) (Lipid products) were used as is. 1,2-Dipalmitoyl-*sn*-glycero-3-phosphocholine-*N,N,N*-trimethyl-*d*₉ (DPPC-*d*₉) was synthesized as reported earlier, and the isotopic purity was found to be better than 98%.⁴⁵ Per-deuterated alkyl chain DPPC (DPPC-*d*₆₂) was purchased from Avanti Polar Lipids Inc. MTSL (1-oxyl-2,2,5,5-tetramethyl-3-pyrroline-3-methyl) methanethiosulfonate was from Toronto Research Chemicals, Ontario, CA. The spin probes 3-(carboxy)-2,2,5, 5-tetramethyl-1-pyrrolidinyloxy (Proxy) and 5-doxyl-stearic acid (5DSA) were purchased from Aldrich. 1,2-dipalmitoyl-*sn*-glycero-3-phospho (TEMPO) choline (HPCSP) and 1-palmitoyl-2-stearoyl-(10-DOXYL)-*sn*-glycero-3-phosphocholine (10PCSP) were purchased from Avanti Polar Lipids Inc. 1-Palmitoyl-2-stearoyl-(5-DOXYL)-*sn*-glycero-3-phosphocholine (5PCSP) was synthesized according to the procedure described earlier.⁴⁶ Materials for peptide synthesis and purification appear in the Supporting Information.

Peptide Synthesis and Labeling. Peptides were synthesized by a solid phase method on rink amide MBHA resin (0.68 mequiv) by using an ABI 433A automatic peptide synthesizer. The principles of peptide-resin cleavage and peptide purification have been described elsewhere,²⁶ and detailed information appears in the Supporting Information. The peptides were labeled with MTSL as reported earlier.² Labeled peptides were shown to be homogeneous by analytical HPLC (>97%, by weight) and were analyzed by electrospray mass spectroscopy. Table 1 lists all of the spin labeled peptides prepared and their designations.

Sample Preparation. A dry phospholipid mixture of DPPC/PG (7:3 w/w), DPPC-*d*₉/PG (7:3 w/w), or DPPC-*d*₆₂/PG (7:3 w/w) was dissolved in a CHCl₃/MeOH mixture (2:1, v/v). Each of the spin labeled phospholipids 5, 10, HPCSP, 5DSA, or Proxy were added from a stock solution to the DPPC/PG (7:3 w/w) or the DPPC-*d*₉/PG (7:3 w/w) solution to give 1% by weight. The solvents were evaporated under a nitrogen stream. A lipid suspension was prepared by vortex and sonication of the lipids in deuterated or nondeuterated phosphate buffer to give a final concentration of 5 mg/mL. Once the sample is fully hydrated, large unilamellar vesicles (LUVs) were prepared by extrusion with an Avastin LiposoFast extruder.⁴⁷ The peptides were added to the LUV solution to give a peptide concentration of 0.16 mM and a peptide–lipid molar ratio of 1/200 in order to ensure maximum binding of the peptides to the LUVs, as determined previously.⁴⁸ The concentration of spin labeled peptides in the water–glycerol (30%) solution was 0.35 mM. All samples for

DEER measurements were prepared in D₂O solutions to extend the phase memory time. Samples for DEER and ESEEM measurements were prepared as follows: after equilibration, approximately 30–40 μ l of each were rapidly frozen by insertion of the EPR tube (2.7 mm i.d. and 3.7 mm o.d.) into liquid nitrogen. Thereafter, the samples remained frozen.

Spectroscopic Measurements. All CW X-band (9.5 GHz) measurements were performed at room temperature (23–25 °C) on a Bruker ELEXSYS 500 spectrometer, using flat cells or a couple of round quartz capillaries (0.6 i.d. \times 0.84 o.d., VitroCom Inc.). ESEEM and DEER experiments were carried out at 50 K on a Bruker ELEXSYS E580 spectrometer (9.5 GHz) using the ER4118X-MS-5X probehead with a split ring resonator (5 mm sample access). The constant time four-pulse DEER experiment⁴⁹ was employed, and the experimental details are given in the Supporting Information. Distance distributions were obtained from the dipolar time evolution data by DeerAnalysis2008 software.⁵⁰ Tikhonov regularization was performed with L curve computation, and the regularization parameter was set to 10, 100, or 1000.

The ESEEM experiments were done using the three-pulse pulse sequence $\pi/2$ - τ - $\pi/2$ - T - $\pi/2$ - τ -echo, with a repetition rate of 3 ms and four-step phase cycle.⁵¹ All measurements were performed at a field corresponding to the maximum echo intensity, and the $\pi/2$ and π microwave pulse lengths were 16 and 32 ns, respectively. The τ -value was optimized for maximum modulation depth ($\tau = 1/(2\nu_1) \sim 224$ ns, where ν_1 is the ²H Larmor frequency). The time interval T was incremented in 20 ns steps starting at 40 ns. Fourier transformation of the ESEEM (FT-ESEEM) trace was carried out as follows: after phase correction and normalization, the background decay of the normalized data was subtracted using a polynomial fit; then, the data was apodized with a Hamming window, and zero filling to 512 points was performed followed by FT and cross-term averaging.⁵² All ESEEM traces were treated identically. The number of accumulations was 30–300 depending on the modulation depth.

We have chosen the intensity of the ²H peak, $I(^2\text{H})$, in the FT-ESEEM as a measure for the modulation depth. The ²H peak is composed of a narrow component due to remote deuterium nuclei and a broad component due to water molecules that form H-bonds with the NO group.²⁵ The data analysis in the present study took into account only the narrow spectral constituent.

Computational Methods

MC simulations of melittin in water and membrane were performed as described previously.^{35,36,53} In brief, melittin was described in a reduced way, in which each amino acid was represented by two sites, corresponding to its α -carbon and side chain. The hydrocarbon region of the membrane was represented as a smooth profile of 30 Å width. A negative surface charge, representing the molecular fraction of PG, was located on both sides of the membrane at a distance of 20 Å from the midplane, corresponding to the location of the lipid phosphate groups.³⁵ To calculate the free energy of the peptide in water and in the membrane, four simulations consisting of 900 000 Monte Carlo cycles were conducted. The total free energy of membrane association (ΔG_{total}) was calculated as the difference between the free energies of a peptide in the aqueous phase and in the membrane, using the following equation.³⁵

$$\Delta G_{\text{total}} = \Delta G_{\text{con}} + \Delta G_{\text{sol}} + \Delta G_{\text{imm}} + \Delta G_{\text{lip}} + \Delta G_{\text{def}} + \Delta G_{\text{coul}} \quad (1)$$

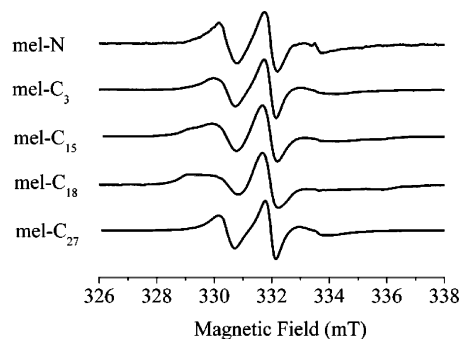


Figure 1. X-band EPR spectra of melittin that is labeled in various positions along the peptide in the presence of LUVs.

In eq 1, ΔG_{con} stands for the change in the free energy due to membrane-induced conformational changes, ΔG_{sol} is the free energy of transfer of the peptide from the aqueous environment to the membrane, ΔG_{imm} accounts for immobilization of the peptide in the membrane, ΔG_{lip} accounts for the free energy due to the change in the conformational freedom of the lipid chains, ΔG_{def} accounts for the membrane deformation associated with peptide incorporation into the membrane, and ΔG_{coul} stands for Coulombic attraction between charged amino acids and the (negative) membrane surface charge. The data of each simulation was used to calculate the tilt angle and penetration depth of the peptide with respect to the membrane plane, and the free energy of membrane association, by averaging over the values obtained in all of the cycles. The penetration depth was calculated as the average over conformations of the distance between the geometric center of the peptide and the membrane midplane. The tilt angle was estimated on the basis of the angle between the peptide's end-to-end vector and the membrane's surface. The reported values are the averages over all of the simulations \pm standard deviations among the values of the different runs.

Melittin's initial structure was taken from Protein Data Bank (PDB) entry 2MLT. Labeling of melittin with MTSL at different positions (Table 1) was mimicked by leucine. This is based on the observation that MTSL is hydrophobic and its free energy of transfer from water into the membrane is very similar to that of leucine.^{36,54} The initial structures of the labeled peptides were obtained by modifying the native structure using the NEST methodology,⁵⁵ with default parameters. The simulations were performed in 30% acidic membranes unless stated otherwise. The helical content of the peptides was calculated as in ref 53.

Experimental Results

CW-EPR Measurements. Figure 1 presents the room temperature CW EPR spectra of the melittin singly labeled mutants in the presence of LUVs. It shows that in the presence of LUVs the label's mobility decreases from the ends of the peptide to its center, with mel-C₁₈ being the most rigid and the N- and C-terminus labels being the most mobile. Comparison of these spectra and the spectra in solution (Figure S1, Supporting Information) shows that the spectra with the LUVs are always considerably broader due to slower tumbling rates, confirming that melittin is bound to the membrane. The spectra of the doubly labeled peptide were approximately a superposition of the spectra of the corresponding singly labeled peptides (Figure S1, Supporting Information).

DEER Measurements—The Reference System. DEER measurements, in the presence and absence of LUVs, were carried out for four double mutants (Table 1). To ensure that

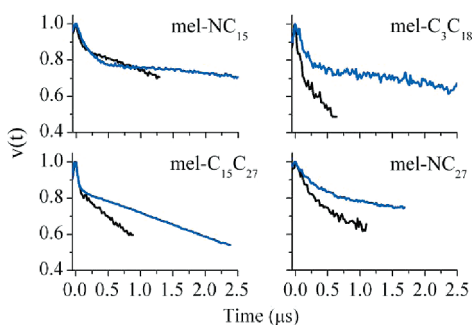


Figure 2. Normalized DEER decays for the doubly labeled melittin peptides within DPPC/PG/D₂O LUVs (black) and in D₂O/30% glycerol solution (blue). The corresponding distance distributions are shown in Figure 3.

the DEER decay (excluding the background decay) obtained from the LUV solutions is owing to intra- and not inter-peptide interactions due to aggregation, we have compared the DEER trace obtained from a singly labeled melittin, mel-C₁₅, with that of a doubly labeled melittin, mel-C₁₅C₂₇ (Figure S2, Supporting Information). The DEER kinetics of mel-C₁₅ could be best fitted with an exponential decay of a dimensionality of 2.14, which is consistent with a two-dimensional distribution of peptide on the LUV surface. The difference between the time domain traces of the singly and doubly labeled peptides clearly showed that, for peptide/phospholipids = 1/200, the dipolar interactions, determined after background subtraction, are intramolecular and that melittin is in a monomeric state.

The time-domain DEER traces of the doubly labeled melittin in solutions with and without LUVs are shown in Figure 2. In all cases, the background decay was significantly faster in the presence of LUVs, although the peptide concentration was lower (0.35 mM vs 0.16 mM, respectively). This is expected because the peptides are not distributed isotropically throughout the solution but are concentrated on the LUVs such that the local concentration is higher than the bulk concentration.⁵⁶ The enhanced contribution of the background decay affected also the signal-to-noise ratio and prevented measurements at long times (Figure S3, Supporting Information).

Figure 3 shows the distance distribution obtained from the DEER measurements in the aqueous phase and in LUV solutions. The fine structures (peaks) appearing in some of the distance distributions are most probably artifacts of the regularization due to noise and should be considered as part of the total width of the distribution. It is evident that, on average, the membrane-bound peptide is shorter than in the aqueous phase, and the overall distance distribution is narrower. The smallest difference was observed for mel-C₁₅C₂₇, where the distance distributions with and without the LUVs are very close. Single-peak distributions were observed in both cases, which are centered on distances of 20 and 22.5 Å, respectively. The distances are similar to the distance between the corresponding α -carbons of Ala15 and Gln26 in the X-ray structure,^{38,39} suggesting that the peptide core is helical even in the aqueous solution. The similarity between the center of the distance distribution of the bound peptides and the corresponding distances in the overall crystal structure (Figure 3) suggests that the average conformation is helical.

While the DEER measurements report the average conformation of melittin in the aqueous phase and in association with LUVs, they do not reveal the penetration depth into the membrane and the orientation of the peptide in the membrane. This information was derived from the ESEEM experiments described next.

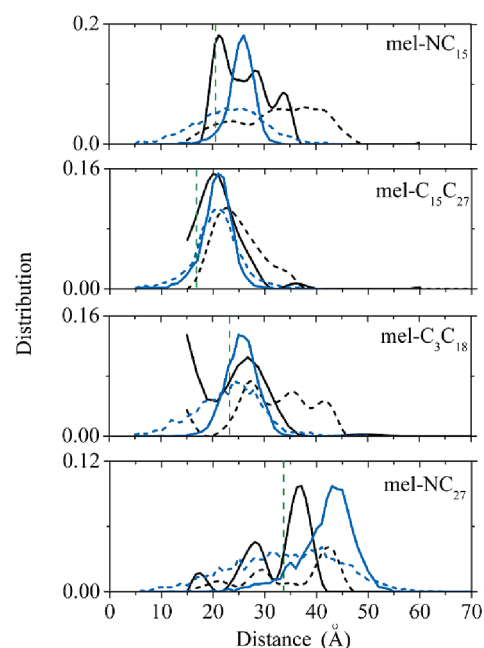


Figure 3. Distance distribution obtained from the DEER traces (black) shown in Figure 2 for the four double mutants studied with (solid) and without (dashed) LUVs. The experimental results were normalized to the maximum of the MC results. The blue (solid and dashed) lines are the results of the MC simulations obtained from the corresponding Leu double mutants. The vertical green line represents the corresponding distance between α -carbons in the crystal structure.^{38,39}

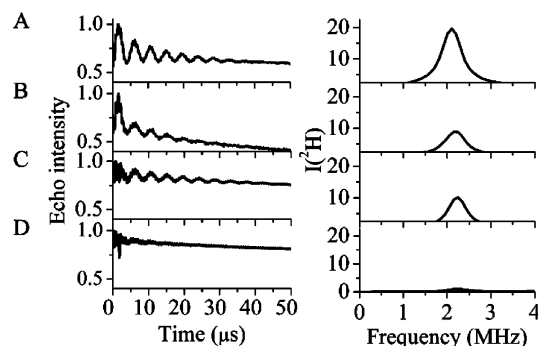


Figure 4. Three-pulse ESEEM time domain traces of mel-C₂₇ in (A) 70% D₂O/30% glycerol, (B) DPPC/PG/D₂O LUVs, (C) DPPC-*d*₆₂/PG LUVs, and (D) DPPC-*d*₉/PG LUVs and their corresponding FT-ESEEM spectra.

ESEEM Measurements—The Reference System. Figure 4 shows examples of time domain ESEEM traces and FT-ESEEM spectra of mel-C₂₇ in a D₂O buffer, with LUVs in a deuterated buffer and with deuterated LUVs. These show the range of ²H modulation depth that can be observed. The modulation depth is expressed in the intensity of the ²H peak in the FT-ESEEM spectrum, given by $I(^2\text{H})$. In general, the larger $I(^2\text{H})$ is, the higher is the ²H density around the spin label. To correlate $I(^2\text{H})$ with the insertion depth of the spin label in the peptide, a proper reference is required.

The reference chosen was spin labeled phospholipid molecules (Figure 5). The spin label in HPCSP senses the polar headgroup region, 5PCSP probes the region below the phosphate group toward the membrane, and 10PCSP the hydrocarbon region. These spin probes were introduced in minute amounts to the phospholipid solutions prior to the preparation of the LUVs. Earlier reports showed that the addition of melittin to DPPC/PG model membranes changed the modulation depth experienced by 5, 7, and 16DSA (doxyl-stearic acid spin

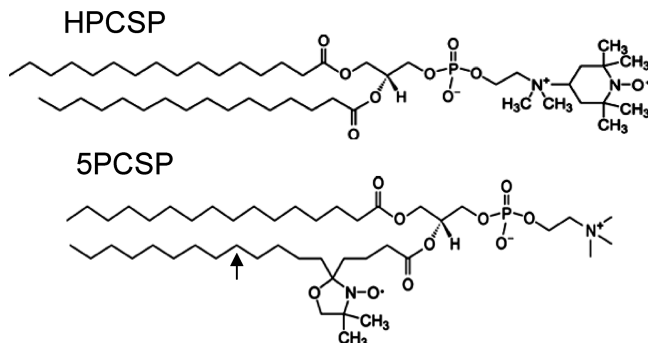


Figure 5. Structures of the HPCSP and 5PCSP spin labeled phospholipids. The 10PCSP probe is similar to 5PCSP with the nitroxide spin label in the position marked by the arrow.

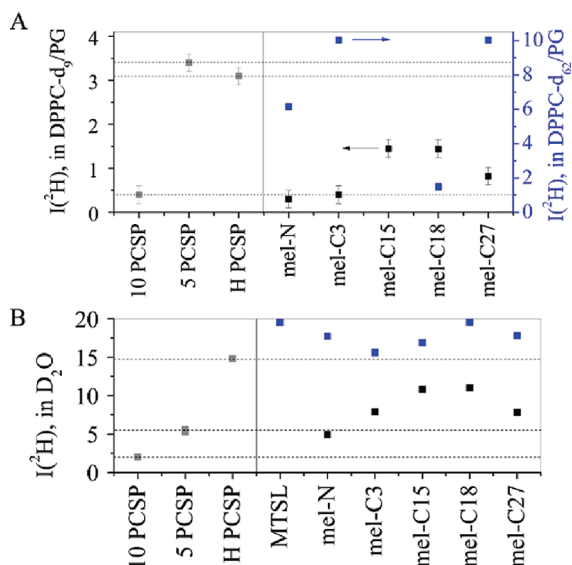


Figure 6. $I(^2\text{H})$ value of labeled melittin within (A) DPPC- d_9 /PG (black squares) and DPPC- d_{62} /PG (blue squares). (B) DPPC/PG/ D_2O LUVs (black squares) compared to the unbound labeled melittin and free MTSL, in 70% D_2O /30% glycerol (blue squares). The spin labeled phospholipids reference in the presence of melittin (gray squares) is also shown for comparison in DPPC- d_9 /PG and DPPC/PG/ D_2O LUVs. The dotted lines indicate the $I(^2\text{H})_{n\text{-PCSP}}$ ($n = \text{H}, 5, 10$) values. The standard errors are marked, but sometimes they are smaller than the symbols.

labels).²⁶ Accordingly, we compared the $I(^2\text{H})$ values of the PCSP spin probes in the various types of deuterated LUV solutions with and without melittin (Figure S4, Supporting Information). Due to a small, but significant observed difference we used the results of the samples with melittin as the reference.

Figure 6 shows the dependence of $I(^2\text{H})$ on the spin-label position in the phospholipids in samples of LUVs/ D_2O and DPPC- d_9 /PG LUVs with melittin (non-labeled). Earlier calculations showed that $I(^2\text{H})$ should exhibit an approximate linear dependence down (or up) to ~ 10 Å from the deuterated layer in DPPC- d_9 /PG LUVs.²⁵ For the deuterated LUVs, the trend $I(^2\text{H})_{\text{HPCSP}} \sim I(^2\text{H})_{\text{5PCSP}} \gg I(^2\text{H})_{\text{10PCSP}} \sim 0$ is observed. The similar values for HPCSP and 5PCSP confirm the bend of the polar headgroup region with respect to the alkyl chain.⁵⁷ For the LUV/ D_2O samples, the trend of $I(^2\text{H})$ is $I(^2\text{H})_{\text{HPCSP}} I(^2\text{H})_{\text{5PCSP}} > I(^2\text{H})_{\text{10PCSP}}$ (Figure 6B). The close $I(^2\text{H})$ values for 5PCSP and 10PCSP are a consequence of the sigmoid shape of the polarity profile within the membrane.²⁵

Orientation and Location of Melittin within the Membrane. A plot of $I(^2\text{H})$ vs the spin label position in the peptide in DPPC- d_9 /PG LUVs is presented in Figure 6A. It shows that

labels in the center of the peptide, attached to C_{15} and C_{18} , have the highest $I(^2\text{H})$ values, while those at the ends show lower values. These results on their own are not sufficient for locating the peptide relative to the membrane because low values of $I(^2\text{H})$ could arise from a residue that is buried in the hydrophobic region of the membrane or is situated in the aqueous phase, not interacting with the membrane at all. Therefore, the $I(^2\text{H})$ values of the spin labeled peptides in LUVs/ D_2O are essential to complement the picture and differentiate these two options. The results are depicted in Figure 6b, demonstrating a trend very similar to that observed with the DPPC- d_9 /PG LUVs.

Figure 6B also shows the dependence of the $I(^2\text{H})$ values of the spin labeled peptides in a D_2O buffer along with that of a free MTSL, which represents the highest possible $I(^2\text{H})$ value. The scatter of the points is much larger than the experimental error and reveals that different residues experience a different water exposure in solution. Here, mel-C₁₈ experiences the largest exposure to water, while mel-C₃, the lowest. The difference between the degrees of water exposure of the amino acids might indicate that melittin is partially structured even in solution. Alternatively, the differences can also be due to exchangeable protons in amino acids in the close vicinity of the label. Upon the addition of LUVs, all peptides exhibit a considerable reduction in $I(^2\text{H})$ of D_2O , confirming the binding to the LUVs.

The combined D_2O , DPPC- d_9 ESEEM results indicate that the spin labels in mel-C₁₈ and mel-C₁₅ are exposed to the solvent, whereas the N- and C-termini are somewhat deeper in the membrane. In order to substantiate this observation, ESEEM measurements were carried out also with DPPC- d_{62} . The results presented in Figure 6A show that, among the labeled peptides, mel-C₁₈ is the furthest away from the hydrophobic region, while the termini are the closest.

Computational Results

Free Energy of Melittin–Membrane Association. We first examined the dependence of the free energy of melittin–membrane association on the lipid composition and the ionic strength. We performed MC simulations of the interaction of melittin with membranes containing different proportions of anionic lipids (Figure S5A, Supporting Information). As anticipated, increasing the fraction of the acidic lipids increased the Coulombic interaction between them and melittin’s basic residues and the magnitude of the free energy of melittin–membrane association, i.e., increased affinity. In contrast, increasing the ionic strength decreased the magnitude of the association free energy of melittin with the membrane, due to the shielding effect of the cations (Figure S5B, Supporting Information).

We then compared the experimentally obtained association free energy of melittin⁵⁸ with unilamellar phosphocholine (zwitterionic) vesicles with the corresponding calculated value of melittin interaction with a neutral membrane. The computed value of -15.1 ± 0.6 kT (Figure S5A, Supporting Information) is slightly lower than the experimental value of about -11.8 to -13.6 kT.⁵⁸ We also compared our results to MD simulations of melittin within a membrane containing 10% anionic (and 90% zwitterionic) lipids.⁵⁹ The free energy value of melittin–membrane association of the MD simulation was -21.7 kT in excellent agreement with the -21.1 ± 0.6 kT value of our MC calculations (Figure S5A, Supporting Information).

It is noteworthy that changes in the proportion of anionic lipids and the ionic strength did not affect melittin’s helicity, penetration depth, and orientation relative to the membrane (Figure S6, Supporting Information).

TABLE 2: Thermodynamic Parameters for the Membrane Association of Native and Modified Melittin, Calculated on the Basis of the MC Simulations^a

peptide designation	z (Å)	tilt (deg)	ΔG_{total} (kT)	ΔG_{conf} (kT)
melittin	18.5 ± 0.1	$93 \pm (<1)$	$-29 \pm (<1)$	$-1 \pm (<1)$
mel-NC ₁₅	17.4 ± 0.1	$96 \pm (<1)$	$-38 \pm (<1)$	$-5 \pm (<1)$
mel-C ₁₅ C ₂₇	$18.2 \pm (<0.1)$	95 ± 1	$-29 \pm (<1)$	$2 \pm (<1)$
mel-C ₃ C ₁₈	17.2 ± 0.1	104 ± 1	$-29 \pm (<1)$	$1 \pm (<1)$
mel-NC ₂₇	$18.5 \pm (<0.1)$	$95 \pm (<1)$	$-37 \pm (<1)$	$-6 \pm (<1)$

^a Each value is represented as an average \pm standard deviation. The penetration depth, z , is calculated as the average distance between the peptide's α -carbon and the membrane midplane. The tilt angle, tilt, is calculated as the angle between the peptide's end-to-end vector and the membrane normal. ΔG_{total} is the total free energy change upon membrane association; ΔG_{conf} stands for the free energy change due to the membrane-induced conformational changes in the peptide (eq 1).

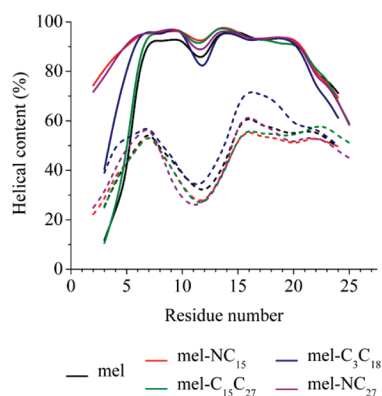


Figure 7. Calculated helical content of native and Leu-modified melittin. The dotted curves show the results of simulations in the aqueous phase, and the continuous curves refer to the membrane simulations. The results obtained with the label (represented as Leu) at different amino acids are plotted using different colors according to the legend.

Native vs Labeled Melittin. We conducted MC simulations of the interactions of native and mutant melittin peptides with model membranes, composed of 30% acidic lipids, and correlated the results with the experimental data presented above (Table 2). In the MC simulations, the interactions between pairs of amino acids are described using statistical (knowledge-based) potentials, derived from known protein structures.⁶⁰ Since there is no data that enables the derivation of similar potential terms for the spin probe, we were forced to represent it as an amino acid. Fortunately, the probe and leucine share very similar polarity and membrane partitioning.^{54,61} Thus, the cysteine side chains with the nitroxide probes, positioned as designated in Table 1, were substituted by leucine in the simulations.

Overall, the native and “labeled” melittin peptides showed the same membrane behavior. They all adsorbed onto the membrane surface at an angle of $93\text{--}103^\circ$ with respect to the membrane normal (Table 2) at an approximately helical conformation (Figure 7), and penetrated into the membrane to the same extent (distance of $17.2\text{--}18.5$ Å from the bilayer midplane; Table 2). Additionally, they all assumed conformations in which the hydrophobic amino acids were embedded in the hydrocarbon region of the membrane and the polar and charged residues interacted with the aqueous phase or the water–membrane interface (Figure 8). Thus, the leucine mutation, representing the spin label, did not appear to alter melittin's mode of interaction with the membrane significantly.

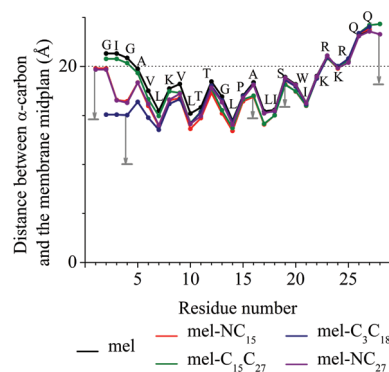


Figure 8. Location of native and mutant melittin near the membrane. The average distance of the α -carbon atoms from the membrane midplane in the MC simulations is shown for each residue. The gray arrows refer to the location of the NO group of the probe (see text). The corresponding rms fluctuations (Figure S7, Supporting Information) indicate that the termini are more flexible than the core, as anticipated.

However, along with the similarities, there are some differences between certain modified peptides and native melittin. For example, the free energy of membrane association of the mel-NC₁₅ and mel-NC₂₇ peptides was larger in magnitude than that of native melittin (Table 2). This is attributed to the free energy change due to membrane-induced conformational changes in the peptide, ΔG_{conf} , while other energetic terms were similar. We therefore investigated the helicity of native melittin and the mutants.

We calculated the helical content of the native and modified peptides in the aqueous phase and in the membrane (Figure 7). As anticipated, the peptides exhibited a significant increase in their helical content upon membrane association. The native and “labeled” peptides sampled similar conformations in the aqueous phase. However, the N-terminus of mel-NC₁₅ and mel-NC₂₇ had higher helical content in the membrane than the rest of the peptides (Figure 7). Since these were the only peptides with an N-terminal “label”, we concluded that the incorporation of a hydrophobic “label” (i.e., a leucine residue) at this position in melittin pulled the N-terminal deeper into the membrane and increased the helicity. This led to an increase of the magnitude of the free energy change due to membrane-induced conformational changes (in the peptide) and the total association free energy of these two peptides in comparison to the rest (Table 2). The analysis of the prevalent conformations of the melittin mutants, presented below, supports this conclusion. In contrast, the incorporation of the “label” into the C-terminus of melittin did not increase the helicity. This is attributed, in part, to the fact that the C-terminus is too polar to partition into the membrane even after the addition of the hydrophobic “probe”.

Melittin Structure, Orientation, and Penetration Depth. Figure 3 shows the distribution of distances between the α -carbon atoms of the “labeled” residues observed in the MC simulations in comparison with the DEER experiments of the various melittin mutants. The experimental and computational results correlate well. The distance distribution is wider in water than in membrane in all cases, which is consistent with the anticipation that, roughly speaking, melittin is a random coil in solution and it becomes ordered upon membrane interaction (Figure 7). Mel-C₁₅C₂₇ showed the least significant broadening of the distance distribution in water relative to membrane, similar to the experiment. This is probably due to the fact that the helical content of the C-terminal is high in water (Figure 7). In general, the agreement between the DEER results and the MC simula-

tions is better for the membrane-associated peptide than for the peptide in solution.

Figure 8 shows the average location of the α -carbon atoms of the amino acids of native and modified melittin within the membrane. As mentioned above, all peptides adsorbed onto the membrane surface in similar conformation, orientation, and location. The C-terminus, containing some charged residues, is exposed to water. In native and in most of the modified melittin peptides, the N-terminus is located in the membrane–water interface. The only exception is mel-C₃C₁₈, for which the incorporation of the “label” (leucine) instead of Gly3 caused deeper penetration of the N-terminus into the membrane as compared to the rest of the peptides. Overall, the MC simulations are qualitatively consistent with the experiments concerning the locations of C₃, C₁₅, and C₁₈ (Figure 6). However, it appears that the termini penetrate deeper into the membrane according to the ESEEM experiments than in the simulations. This discrepancy will be discussed next.

Discussion

In the following, we first discuss the implications and current limitations of the ESEEM techniques for deriving peptide insertion depth in membranes. This is followed by a discussion of the restrictions of the MC simulations. We then depict the results of the combined approach that helps to reduce the limitations of each technique separately.

Implications and Limitations of the ESEEM Technique.

In order to estimate the insertion depth of the peptide into the membrane from the $I(^2\text{H})$ values, we used references based on spin labeled phospholipids. The comparison of the reference spin probes in LUVs/D₂O and DPPC-*d*₉ LUVs leads to conflicting results regarding the insertion depth. The DPPC-*d*₉ LUV measurements suggest a deeper penetration depth than the D₂O results (Figure 6), although overall, both give the same melittin conformation. It is worth mentioning that a similar conflict was observed in our earlier study that focused on mel-N only.²⁶ To reconcile the discrepancy, we then suggested that the N-terminus is close to the membrane surface region and adapts a conformation where the spin label at the N-terminus has limited water exposure. However, this explanation is inconsistent with the more complete data set presented above. We think that the reason for this inconsistency is that spin labeled phospholipids are not a proper reference system for deuterated LUVs. Problems in using labeled lipids in accessibility studies were previously pointed out by Nielsen et al.⁶ These were associated with wide variations in the probe conformation that complicated interpretation, and the disorder that may be introduced by the label, especially near the bilayer midplane. In addition, spin labeled lipids cannot account for the changes in the modulation depth associated with the volume of the peptide and the excluded volume associated with it. The volume of spin labeled melittin may change the number of phospholipid molecules in the vicinity of its spin label, thus effectively reducing their local density in this region. This would lead to lower $I(^2\text{H})$ values, which are misinterpreted as a deeper penetration. D₂O molecules, on the other hand, are small and mobile, and they should be less affected by the excluded volume. We therefore consider the D₂O reference to be more reliable. Accordingly, the spin labels in mel-C₁₅ and mel-C₁₈ are not buried deeper than position 5 of the phospholipid (Figure 6). This is also supported by the MC simulation. The simulation shows that the α -carbon of Ser18 is ~ 18 Å from the membrane midplane (Figure 8), which is above the fifth position in the alkyl chain. Although we have accounted for changes in D₂O

distribution in the membrane due to the insertion of melittin by using as a reference spin labeled phospholipids in LUVs in the presence of melittin, possible contributions to the modulation depth from exchangeable protons of the backbone and in side chains were not considered. For example, in a recent study, modulations due to D₂O were observed for a buried residue in a membrane protein.⁶² The above reservations call for a search for a better reference system, free from the above concerns. One possibility would be a transmembrane helix, as used by Nielsen et al.⁶

The penetration depth of spin labeled peptides/proteins into membranes is commonly obtained by the combined effect of paramagnetic quenchers situated selectively in the solvent and hydrophobic regions.^{6,20,63} In principle, the ESEEM methodology presented here provides the same type of information. However, there are two principal advantages. First, the data is derived directly from interactions between peptides and deuterated membrane and not through the effect of a “third party”, namely, the quencher. While per-deuterated lipids may differ from the protonated counterpart,⁶⁴ the use of specifically deuterated lipids, like DPPC-*d*₉, is more innocent because only a few protons are replaced. A second advantage is that the modulation depth can be analyzed quantitatively. We have already reported a simple model for such an analysis,²⁶ but it should be tested against a known good reference system for calibration. Two disadvantages of the ESEEM approach are that it requires frozen solutions, similar to DEER, and the use of specifically deuterated membranes, which is costly and requires special synthetic efforts.

The secondary structure of peptides/proteins in membranes, particularly helices, can be determined by solid state NMR of aligned samples using the PISEMA method.⁶⁵ The major advantage of this method is that it is label free; namely, no chemical modifications are involved, and one sample provides the information needed as opposed to the EPR methodology that requires the preparation of many mutants. Some disadvantages relative to the DEER/ESEEM approach are the much lower sensitivity, 3–9 mM of protein are required in NMR⁶⁶ as compared to 0.1–0.2 mM in EPR, and the need for well oriented samples which complicates sample preparation.

Limitations of the MC Simulations. The free energy component that described the (membrane-induced) conformational changes in the peptide is derived from the proteins' three-dimensional structures, and includes only native amino acids.⁶⁰ However, the EPR techniques included labeling of melittin with MTSL. As the spin probe could not have been taken into account, it was approximated by a leucine residue of comparable hydrophobicity.^{54,61} Consequently, the length of the probe and its other unique characteristics were not taken into consideration in the model.

An additional limitation of the model is related to the implicit description of the peptide, where each residue is represented by two interaction sites. The simplicity makes the simulations computationally feasible. However, it involves inaccuracies in the calculations, especially those related to the solvation free energy (eq 1), which strongly depends on the location of each atom. Moreover, the reduced representation leads to undefined torsion angles of the two residues at both ends of the peptide. This results in an increased flexibility of the chain ends and reduction of the stability of the α -helical conformation in the terminal segments. Accordingly, the helical content is reduced, causing desolvation of the termini. This limitation could be the reason for the discrepancy between experiment and computation regarding the peptide termini (see below).

Experimental vs Computational Results. There is good correlation between the EPR results and the MC simulations concerning the mobility. Both methods show that in the membrane-associated state the peptide ends are significantly more mobile than the core (see Figure S7 (Supporting Information), which shows the rms fluctuations of the α -carbon atoms).

The experimentally obtained distance distributions correlated well with those of the MC simulations (Figure 3). Both show a considerable narrowing of the distributions upon membrane binding. For mel-C₁₅C₂₇, however, the change was relatively small. There is also good agreement between the experimental data and simulation concerning the average distance between the α -carbon atoms (Figure 3). However, in the aqueous phase, the experimentally determined average distances are somewhat higher than the predicted values (Figure 3). Naturally, the distance measured between two MTSL labels is not the same as that determined from the α - (or β -) carbon atoms in the native peptide due to the length and the motional freedom of the label. A recent comparison of distances measured by EPR and the corresponding distances between the β -carbon atoms obtained from the crystal structures of T4-lysozyme and a comparative model of α A-crystallin showed that the difference may vary between -4 and 12 Å with an average of about $0-4$ Å.⁶⁷ Thus, the anticipation is that the measured distances between labels would appear inflated in the aqueous solution compared to the membrane, where the peptide is, in essence, restricted to the helical state.

The experimental distance distribution of mel-C₃C₁₈ is high at $r = 15-20$ Å (Figure 3) which is not reproduced by the MC simulation. This sample was the hardest to measure in terms of signal-to-noise ratio, and therefore, it was acquired for the shortest decay time. It could be that the short distances observed are artifacts due to difficulties associated with the removal of background.

Finally, we discuss the peptide orientation and location within the membrane. The MC simulations yielded an average structure of a continuous α -helix with relatively disrupted termini (Figure 7). The overall conformation is “banana-shaped” with the helix core embedded in the membrane and the termini exposed to the water/lipid polar headgroups (Figure 8). There is a rather good agreement with the ESEEM results in the relative penetration depth of mel-C₃, C₁₅, and C₁₈, while there is some disagreement regarding the N- and C-termini. In comparison to the MC simulations, the ESEEM results suggest a deeper penetration of the termini.

An earlier molecular dynamics simulation showed that MTSL has a clear hydrophobic bias.⁶⁸ Thus, when facing the membrane, the nitrogen of the probe protrudes about $5-6$ Å deeper than the α -carbon atom of the labeled residue.⁶⁸ Conversely, because of steric hindrance, a probe that is introduced at the water-accessible side of the helix would insert only about 2 Å deeper into the membrane than the α -carbon atom. Accordingly, to account for this hydrophobic bias, we added $2-6$ Å to the predicted depth of the α -carbon atoms depending on their location on the helix (Figure 8, gray arrows). Nevertheless, this correction was not sufficient to account for the discrepancy regarding the location of the N- and C-termini spin labels. The discrepancy can be due to either some uncertainties in the MC simulation regarding the peptide ends, as discussed above, or some additional bias of the spin labeling at the peptide ends. This suggests that spin labeling at the ends of the peptide may not be as innocent as desired.

Since the termini appeared to be mobile both in experiment and in simulation, and because of the high energy penalty associated with the transfer of the polar/charged termini from the aqueous phase into the membrane, we suggest that in the

native peptide they reside somewhere in the polar headgroup region of the membrane.

Conclusions

We have presented an approach that combines pulse EPR techniques and MC simulations to obtain the population and prevalent conformation, location, and orientation of membrane-bound peptides. The approach was demonstrated on melittin within a negatively charged membrane. We found that at the peptide/phospholipids ratio of 1:200 melittin is in a monomeric state and adapts an α -helical conformation, primarily parallel to the membrane surface. The obtained configuration of melittin in the membrane is characterized by polar and charged residues facing the solvent, whereas the hydrophobic amino acids penetrate deeper into the membrane. In solution, melittin is mostly disordered, though its C-terminus does have some helical character. We obtained a very good agreement between the distance distributions and the penetration depth of the residues in the peptide core. However, the experimental results showed deeper membrane penetration of the N- and C-termini than predicted by the MC simulations. This could arise from specific effects of the spin labels or from inaccuracies of the MC simulations in the peptide ends. Nevertheless, the experimental results and simulations correlate very well. Their combination provides detailed and more inclusive results that are in agreement with previous findings. Therefore, this approach can be used for further investigation of peptide–membrane interactions. Furthermore, MC simulations may be used to guide the design of EPR experiments both for phrasing of testable hypotheses regarding the structure of the peptide in the aqueous phase and the membrane, and by suggesting the optimal residues for spin labeling.

Acknowledgment. This work was supported, in part, by the ISF-VATAT Converging technologies program, by the Minerva Foundation (D.G.), and by the European Commission under the sixth Framework Programme through the Marie-Curie Action: BIOCONTROL, contract number MCRTN - 33439 (N.B.-T., Y.G.). D.G. holds the Erich Klieger Professorial chair in Chemical Physics.

Supporting Information Available: Peptide synthesis details. Six figures showing X-band EPR spectra of melittin, DEER traces and distance distributions obtained from the singly and doubly labeled melittin, normalized DEER decays after background removal for the doubly labeled melittin peptides, the $I(^2\text{H})$ values of the spin probes examined in this work in deuterated membranes and D₂O with and without melittin, the calculated free energy of melittin–membrane association as a function of the fraction of anionic lipids (at a constant ionic strength of 0.1 M) and the ionic strength, and calculated rms fluctuations of the α -carbon atoms of native melittin in association with a membrane. This material is available free of charge via the Internet at <http://pubs.acs.org>.

Note Added after Print Publication. This paper was published on the Web on September 2, 2009, and in the September 24, 2009, issue. Due to a production error, Figures 7 and 8 were incorrect. The electronic version was corrected and reposted to the Web issue on October 14, 2009. An Addition and Correction was also published (DOI: 10.1021/jp909559d).

References and Notes

- (1) Steinhoff, H. J. *Front. Biosci.* **2002**, *7*, c97.
- (2) Hubbell, W. L.; Gross, A.; Langen, R.; Lietzow, M. A. *Curr. Opin. Struct. Biol.* **1998**, *8*, 649.

- (3) Fanucci, G. E.; Cafiso, D. S. *Curr. Opin. Struct. Biol.* **2006**, *16*, 644.
- (4) Anbazhagan, V.; Vijay, N.; Kleinschmidt, J. H.; Marsh, D. *Biochemistry* **2008**, *47*, 8414.
- (5) Steinhoff, H.; Savitsky, A.; Wegener, C.; Pfeiffer, M.; Plato, M.; Mobius, K. *Biochim. Biophys. Acta* **2000**, *1457*, 253.
- (6) Nielsen, R. D.; Che, K.; Gelb, M. H.; Robinson, B. H. *J. Am. Chem. Soc.* **2005**, *127*, 6430.
- (7) Hustedt, E. J.; Beth, A. H. *Biological Magnetic Resonance: Structural information from CW-EPR spectra of dipolar coupled nitroxide spin labels*, 2000.
- (8) Han, X.; Bushweller, J. H.; Cafiso, D. S.; Tamm, L. K. *Nat. Struct. Biol.* **2001**, *8*, 715.
- (9) Steinhoff, H. *J. Biol. Chem.* **2004**, *385*, 913.
- (10) Hubbell, W. L.; Cafiso, D. S.; Altenbach, C. *Nat. Struct. Biol.* **2000**, *7*, 735.
- (11) Altenbach, C.; Greenhalgh, D. A.; Khorana, H. G.; Hubbell, W. L. *Proc. Natl. Acad. Sci. U.S.A.* **1994**, *91*, 1667.
- (12) Schiemann, O.; Prisner, T. F. *Q. Rev. Biophys.* **2007**, *40*, 1.
- (13) Jeschke, G.; Polyhach, Y. *Phys. Chem. Chem. Phys.* **2007**, *9*, 1895.
- (14) Borbat, P. P.; Freed, J. H. *Methods Enzymol.* **2007**, *423*, 52.
- (15) Milov, A. D.; Erilov, D. A.; Salnikov, E. S.; Tsvetkov, Y. D.; Formaggio, F.; Toniolo, C.; Raap, J. *Phys. Chem. Chem. Phys.* **2005**, *7* (8), 1794.
- (16) Salnikov, E. S.; Erilov, D. A.; Milov, A. D.; Tsvetkov, Y. D.; Peggion, C.; Formaggio, F.; Toniolo, C.; Raap, J.; Dzuba, S. A. *Biophys. J.* **2006**, *91*, 1532.
- (17) Hustedt, E. J.; Beth, A. H. *Biological Magnetic Resonance*, 2000, *19*; Eds. Berliner, L. J., Eaton, S. S., Eaton, G. R., Eds.; Kluwer Academic/Plenum Publishers: New York; pp 155.
- (18) Drescher, M.; Veldhuis, G.; van Rooijen, B. D.; Milikisyan, S.; Subramaniam, V.; Huber, M. *J. Am. Chem. Soc.* **2008**, *130*, 7796.
- (19) Georgieva, E. R.; Ramlall, T. F.; Borbat, P. P.; Freed, J. H.; Eliezer, D. *J. Am. Chem. Soc.* **2008**, *130*, 12856.
- (20) Jao, C. C.; Hegde, B. G.; Chen, J.; Haworth, I. S.; Langen, R. *Proc. Natl. Acad. Sci. U.S.A.* **2008**, *105*, 19666.
- (21) Dikanov, S. A.; Tsvetkov, Y. D. *Electron Spin Echo Envelope Modulation (ESEEM) Spectroscopy*; CRC Press: Boca Raton, FL, 1992.
- (22) Kevan, L.; Schwartz, R. N. Modulation of electron spin-echo decay in solids. *Time domain electron spin resonance*; John Wiley & Sons: New York, 1979; p 279.
- (23) Schweiger, A.; Jeschke, G. Nuclear modulation effect I: basic experiments. *Principles of pulse electron paramagnetic resonance*; Oxford University Press: New York, 2001.
- (24) Bartucci, R.; Erilov, D. A.; Guzzi, R.; Sportelli, L.; Dzuba, S. A.; Marsh, D. *Chem. Phys. Lipids* **2006**, *141*, 142.
- (25) Erilov, D. A.; Bartucci, R.; Guzzi, R.; Shubin, A. A.; Maryasov, A. G.; Marsh, D.; Dzuba, S. A.; Sportelli, L. *J. Phys. Chem. B* **2005**, *109*, 12003.
- (26) Carmieli, R.; Papo, N.; Zimmermann, H.; Potapov, A.; Shai, Y.; Goldfarb, D. *Biophys. J.* **2006**, *90*, 492.
- (27) Milik, M.; Skolnick, J. *Proteins* **1993**, *15*, 10.
- (28) Baumgartner, A. *Biophys. J.* **1996**, *71*, 1248.
- (29) Ducarme, P.; Rahman, M.; Brasseur, R. *Proteins* **1998**, *30*, 357.
- (30) Efremov, R. G.; Nolde, D. E.; Vergoten, G.; Arseniev, A. S. *Biophys. J.* **1999**, *76*, 2448.
- (31) Maddox, M. W.; Longo, M. L. *Biophys. J.* **2002**, *82*, 244.
- (32) Veresov, V. G.; Davidovskii, A. I. *Eur. Biophys. J.* **2007**, *37*, 19.
- (33) Tzliil, S.; Murray, D.; Ben-Shaul, A. *Biophys. J.* **2008**, *95*, 1745.
- (34) Wee, C. L.; Sansom, M. S.; Reich, S.; Akhmatkaya, E. *J. Phys. Chem. B* **2008**, *112*, 5710.
- (35) Shental-Bechor, D.; Haliloglu, T.; Ben-Tal, N. *Biophys. J.* **2007**, *93*, 1858.
- (36) Kessel, A.; Shental-Bechor, D.; Haliloglu, T.; Ben-Tal, N. *Biophys. J.* **2003**, *85*, 3431.
- (37) Habermann, E. *Science* **1972**, *177*, 314.
- (38) Terwilliger, T. C.; Eisenberg, D. *J. Biol. Chem.* **1982**, *257*, 6010.
- (39) Terwilliger, T. C.; Eisenberg, D. *J. Biol. Chem.* **1982**, *257*, 6016.
- (40) Brown, L. R.; Braun, W.; Kumar, A.; Wuthrich, K. *Biophys. J.* **1982**, *37*, 319.
- (41) Inagaki, F.; Shimada, I.; Kawaguchi, K.; Hirano, M.; Terasawa, I.; Ikura, T.; Go, N. *Biochemistry* **1989**, *28*, 5985.
- (42) Okada, A.; Wakamatsu, K.; Miyazawa, T.; Higashijima, T. *Biochemistry* **1994**, *33*, 9438.
- (43) Lam, Y. H.; Wassall, S. R.; Morton, C. J.; Smith, R.; Separovic, F. *Biophys. J.* **2001**, *81*, 2752.
- (44) Raghuraman, H.; Chattopadhyay, A. *Biosci. Rep.* **2007**, *27*, 189.
- (45) Eibl, H. *Proc. Natl. Acad. Sci. U.S.A.* **1978**, *75*, 4074.
- (46) Fellmann, P.; Zachowski, A.; Devaux, P. F. *Methods Mol. Biol.* **1994**, *27*, 161.
- (47) MacDonald, R. C.; MacDonald, R. I.; Menco, B. P.; Takeshita, K.; Subbarao, N. K.; Hu, L. R. *Biochim. Biophys. Acta* **1991**, *1061*, 297.
- (48) Papo, N.; Shai, Y. *Biochemistry* **2003**, *42*, 458.
- (49) Pannier, M.; Veit, S.; Godt, A.; Jeschke, G.; Spiess, H. W. *J. Magn. Reson.* **2000**, *142*, 331.
- (50) Jeschke, G.; Chechik, V.; Ionita, P.; Godt, A.; Zimmermann, H.; Bahman, J.; Timmel, C. R.; Hilger, D.; Jung, H. *Appl. Magn. Reson.* **2006**, *30* (3–4), 473.
- (51) Fauth, J. M.; Schweiger, A.; Braunschweiler, L.; Forrer, J.; Ernst, R. R. *J. Magn. Reson.* **1986**, *66*, 74.
- (52) Van Doorslaer, S.; Sierra, G. A.; Schweiger, A. *J. Magn. Reson.* **1999**, *136*, 152.
- (53) Shental-Bechor, D.; Kirca, S.; Ben-Tal, N.; Haliloglu, T. *Biophys. J.* **2005**, *88*, 2391.
- (54) Yu, Y. G.; Thorgeirsson, T. E.; Shin, Y. K. *Biochemistry* **1994**, *33*, 14221.
- (55) Petrey, D.; Xiang, Z.; Tang, C. L.; Xie, L.; Gimpelev, M.; Mitros, T.; Soto, C. S.; Goldsmith-Fischman, S.; Kernysky, A.; Schlessinger, A.; Koh, I. Y.; Alexov, E.; Honig, B. *Proteins* **2003**, *53*, 430.
- (56) Ruthstein, S.; Goldfarb, D. *J. Phys. Chem. C* **2008**, *112* (18), 7102.
- (57) Zanker, P. P.; Jeschke, G.; Goldfarb, D. *J. Chem. Phys.* **2005**, *122*, 024515.
- (58) Ladokhin, A. S.; White, S. H. *Biochim. Biophys. Acta* **2001**, *1514*, 253.
- (59) Lazaridis, T. *Proteins* **2005**, *58*, 518.
- (60) Bahar, I.; Jernigan, R. L. *J. Mol. Biol.* **1997**, *266*, 195.
- (61) Sammalkorpi, M.; Lazaridis, T. *Biophys. J.* **2007**, *92*, 10.
- (62) Volkov, A.; Dockter, C.; Bund, T.; Paulsen, H.; Jeschke, G. *Biophys. J.* **2009**, *96*, 1124.
- (63) Macosko, J. C.; Kim, C. H.; Shin, Y. K. *J. Mol. Biol.* **1997**, *267*, 1139.
- (64) Aussenac, F.; Laguerre, M.; Schmitter, J. M.; Dufourc, E. J. *Langmuir* **2003**, *19*, 10468.
- (65) Opella, S. J.; Nevzorov, A.; Mesleb, M. F.; Marassi, F. M. *Biochem. Cell Biol.* **2002**, *80*, 597.
- (66) De Angelis, A. A.; Howell, S. C.; Nevzorov, A. A.; Opella, S. J. *J. Am. Chem. Soc.* **2006**, *128*, 12256.
- (67) Alexander, N.; Bortolus, M.; Al-Mestarihi, A.; McHaourab, H.; Meiler, J. *Structure* **2008**, *16*, 181.
- (68) Sammalkorpi, M.; Lazaridis, T. *Biochim. Biophys. Acta* **2007**, *1768*, 30.